Manifold Diffusion Geometry: Curvature, Tangent Spaces, and Dimension

Iolo Jones Durham University

November 2024

Abstract

We introduce novel estimators for computing the curvature, tangent spaces, and dimension of data from manifolds, using tools from diffusion geometry. Although classical Riemannian geometry is a rich source of inspiration for geometric data analysis and machine learning, it has historically been hard to implement these methods in a way that performs well statistically. Diffusion geometry lets us develop Riemannian geometry methods that are accurate and, crucially, also extremely robust to noise and low-density data. The methods we introduce here are comparable to the existing state-of-the-art on ideal dense, noise-free data, but significantly outperform them in the presence of noise or sparsity. In particular, our dimension estimate improves on the existing methods on a challenging benchmark test when even a small amount of noise is added. Our tangent space and scalar curvature estimates do not require parameter selection and substantially improve on existing techniques.

Contents

1	Introduction	1
2	Geometry background	3
3	Computing the dimension, tangent space, and curvature	5
4	Dimension estimation	8
5	Tangent space estimation	10
6	Curvature estimation	11
7	Conclusions	13

1 Introduction

For many problems in geometric and topological data analysis, we can safely assume that the data lie on a manifold. This assumption is called the 'manifold hypothesis' and means that the classical theory of Riemannian geometry can, in principle, be applied to the problem. However, on a manifold, it is possible to take limits of quantities, and so define derivatives, vector fields, integrals, and all the other calculus tools that give Riemannian geometry its power. Applying this paradigm directly to data is hard: a finite data set is discrete, so limits cannot exist in the same way, and real-world data is often noisy.

This paper introduces a range of novel techniques for manifold data, using the theory of diffusion geometry [25]. Diffusion geometry recasts the classical theory of Riemannian geometry in terms of the 'heat flow' on the manifold, which is an example of a stochastic process called a Markov diffusion. Markov diffusion processes provide extremely robust statistics and powerful computational tools: they have recently underpinned the development of generative image and video artificial intelligence models [30, 23, 31], and there are many well-developed techniques for estimating the heat flow on a manifold [13, 8]. By estimating the heat flow from data we obtain an estimate for the Laplacian operator Δ , and with it can construct most

of the important objects in Riemannian geometry. In particular, we will construct new estimators for the tangent spaces to the manifold, the dimension of the manifold at each point and also globally, and the Riemann, Ricci, and scalar curvatures (see Figure 1). These inherit the excellent statistical properties of the underlying Markov diffusion, and so are extremely robust to noise, outliers, and low sample density.

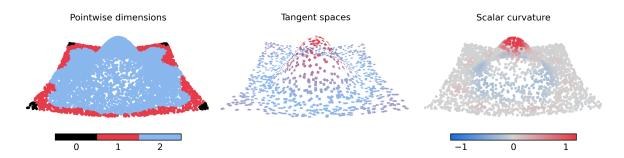


Figure 1: The pointwise dimensions, tangent spaces, and scalar curvature of a manifold

The problems of dimension and tangent space estimation are very well studied: we compare our estimates to the state-of-the-art and find that, for *high quality* data where the sample is large and the noise level is low, our methods achieve comparable results, but, crucially, for *low quality* sparse and noisy data, our methods significantly outperform all existing approaches. There is comparatively little literature on curvature estimation: our method is (to our knowledge) only the third to compute scalar curvature on a general manifold [32, 21], the second to compute the Ricci curvature [2], and the first to compute the Riemann curvature. In quantitative comparisons, we again find that, although similar on extremely dense and clean data, our new diffusion geometry estimators significantly outperform the others when faced with lower density and even small amounts of noise.

1.1 Avoiding the 'hard neighbourhood' paradigm

Most existing techniques for computational geometry and topology use combinatorial objects like graphs or simplicial complexes as a model for geometry. In other words, they resolve the paradox of defining limits on data by defining a 'neighbourhood' to a point as the set of all points within some given distance. This can be used to measure global geometry or topology, or local data like tangents and the Hessian through linear regression on the neighbourhood. A strong theme that emerges consistently throughout this work is that methods like these contain two inherent issues:

- 1. There is a hard cut-off for the edge of a neighbourhood, so points move into and out of each other's neighbourhoods discontinuously. It is, therefore, hard to make these methods robust to noise.
- 2. There is a trade-off between precision (by taking a smaller neighbourhood) and robustness to noise (by taking a larger neighbourhood). This trade-off is usually controlled by a parameter which must be set by the user (and is quantified in [27]).

We will call this approach the hard neighbourhood paradigm. Some hard neighbourhood methods, like most of the existing dimension estimation techniques we test below, as well as persistent homology [28, 14, 33], mitigate the second issue by measuring behaviour over a range of neighbourhood sizes. This improves performance and can guarantee continuity [12], but does not avoid the inherently poor robustness of hard neighbourhoods, as we saw for persistent homology in [25], and as we will see repeatedly below.

Conversely, diffusion geometry encodes the 'locality' information in the Gaussian heat kernel (the transition probability of the diffusion process). Rather than setting a hard cut-off for the edge of a neighbourhood, the kernel smoothly incorporates all the data into and out of consideration, which makes it far more robust to noise. The kernel does have a bandwidth parameter for the size of the 'neighbourhood', but, because the neighbourhood is soft, its exact size is not nearly as important. We will use *variable bandwidth* kernels with straightforward automatic parameter selection, and so will suffer from neither of the two problems outlined above. Our methods are then effectively parameter-free, and highly robust to noise while still being very accurate.

In the infinite-data limit the *hard neighbourhood* and *soft neighbourhood* paradigms converge, but, as statistics on finite data, they are radically different.

1.2 Apology for low intrinsic dimensions

Even though the methods presented here are valid in any dimension, we will only test and exemplify them on manifolds of at most 3 dimensions. This is partly because almost all real geometric data is at most 3-dimensional. Mainly, however, it is because this paper is about *robust* geometric inference in the presence of noise and outliers, and the extent to which we can tell the signal from the noise depends on the density of the data.

For example, a circle could clearly be identified from a sample of 50 points even with significant noise because 50 points are a dense enough sample for a circle. One could probably identify a sphere from a sample of 50 points, but this analysis would not survive the addition of much noise at all, because, for a 2-dimensional object, a sample of 50 points is suddenly far too sparse. It would take a similar density of data, perhaps $50^2 = 2,500$ points, to achieve the same level of certainty as 50 points provided for the circle. Robust geometric inference for a 3-sphere already seems unrealistic, needing perhaps $50^3 = 125,000$ data. This exponential growth means the very question of robust geometric inference is only meaningful when the intrinsic dimension is low: it is 'cursed by dimensionality'.

Many methods (some of which are discussed below) can, for example, precisely identify a 20-dimensional manifold as such in a 50-dimensional ambient space. We will not address this kind of question here, because, we argue, it could never realistically be asked of data with any amount of noise. The ambient dimension may be very high, but the *intrinsic dimension* will always be low. The same limitations apply to the Ricci and Riemann curvatures, which only contribute new information in dimensions 3 and 4: the smallest nontrivial use case for Ricci would be a 3-dimensional manifold embedded in 4-dimensional space. We introduce estimators for these two curvatures, but, given this curse of dimensionality, they are probably not going to be very useful.

1.3 Is the manifold hypothesis reasonable, and does it matter?

The theory of diffusion geometry uses Markov diffusions to extend the familiar Riemannian geometry beyond manifolds to more general probability spaces. Part of the motivation for this was that most of the time in practice, the manifold hypothesis is an unrealistic expectation. One of the main reasons is that manifolds have a constant integer dimension everywhere, which can hardly be said of most real data (whatever 'dimension' is taken to mean for data). Manifolds also cannot have 'branches', like three lines meeting at a point or three planes meeting in a line. However, the methods described here and the Laplacian estimation that underpins them (as well as all the existing hard neighbourhood methods discussed) are only defined locally, so will still apply to non-manifold data wherever that data looks locally like a manifold. As such, the manifold hypothesis need only be a metaphor, because the methods discussed here can, informally, be applied more generally.

1.4 Paper layout

In Section 2 we review the necessary background in Riemannian geometry, and in Section 3 we use the Laplacian Δ to describe estimators for the objects mentioned above. In Sections 4, 5, and 6 we compute examples and comparative tests of each method.

The code for the methods and examples in this paper is available at https://github.com/Iolo-Jones/ManifoldDiffusionGeometry.

2 Geometry background

In modern differential geometry, manifolds \mathcal{M} are usually defined intrinsically (just in terms of measurements made within \mathcal{M}) and any embedding of \mathcal{M} into \mathbb{R}^D is viewed as additional structure. However, in data science, we usually encounter manifolds already embedded in \mathbb{R}^D , and can only infer the intrinsic geometry from the extrinsic geometry. In this sense, the extrinsic perspective is more natural here, and we will develop tools in this paper using the extrinsic definitions of geometric objects, which we now review.

2.1 Tangent spaces and the metric

Suppose $\mathcal{M} \subseteq \mathbb{R}^D$ is a d-dimensional submanifold of \mathbb{R}^D (when d=2 we call \mathcal{M} a surface). A point $p \in \mathcal{M}$ has a tangent space $T_p\mathcal{M}$, corresponding to a d-dimensional linear subspace of \mathbb{R}^D . We can equip the tangent space with an inner product g by setting $g(\vec{v}, \vec{w}) = \vec{v} \cdot \vec{w}$ for all tangent vectors $\vec{v}, \vec{w} \in T_p\mathcal{M}$. This inner product is called the *induced metric* (or the *first fundamental form* when \mathcal{M} is a surface) and turns \mathcal{M} into an *isometrically embedded* Riemannian submanifold of \mathbb{R}^D .

2.2 Curvature of hypersurfaces

We first define the curvature of \mathcal{M} in the simpler case that \mathcal{M} is a hypersurface (i.e. d+1=D) so has, up to sign, a single unit normal \vec{n}_p at each $p \in \mathcal{M}$. If $f: \mathcal{M} \to \mathbb{R}$ is a function and X,Y are vector fields, we can define the Hessian $H(f)(X,Y) := X(Y(f)) - (\nabla_X Y)(f)$. This generalises the matrix of second derivatives

$$\left(\frac{\partial^2 f}{\partial x_i \partial x_i}\right)_{i,j}$$

for functions on Euclidean space, and measures the 'curvature' of the function f with respect to \mathcal{M} . If we let n_p denote the function on \mathcal{M} given by $q \mapsto \vec{n}_p \cdot q$, then, near p, the manifold \mathcal{M} is locally diffeomorphic to the graph of the function n_p , and we can characterise the curvature of \mathcal{M} in terms of the Hessian $H_p(n_p)$. The Hessian is trilinear in f, X, Y, so H(f) is a quadratic form on $T_p\mathcal{M}$ for each $p \in \mathcal{M}$ (it is a $d \times d$ symmetric matrix).

In high dimensions, the geometry is fully characterised by the *Riemann curvature tensor*, which, if X, Y, Z are vector fields, is an operator $Z \mapsto R(X, Y)Z$. For our purposes, we define it through the *Gauss equation*

$$g(R(X,Y)Z,W)(p) = H_p(n_p)(X,Z)H_p(n_p)(Y,W) - H_p(n_p)(Y,Z)H_p(n_p)(X,W).$$

Notice that this equation is unchanged if we instead took the opposite unit normal $-\vec{n}_p$. This equation relates the intrinsic curvature of \mathcal{M} (measured by R) to the curvature of the ambient coordinate functions as viewed from within \mathcal{M} (measured by $H_p(n_p)$). If we let x_i be local coordinates near p such that $\nabla_p x_i$ are an orthonormal basis for the tangent space $T_p \mathcal{M}$ and set

$$R_{ijkl} = g(R(\nabla x_i, \nabla x_j) \nabla x_k, \nabla x_l)(p)$$
 $\alpha_{ij} = H_p(n_p)(\nabla_p x_i, \nabla_p x_j)$

then we get

$$R_{ijkl} = \alpha_{ik}\alpha_{jl} - \alpha_{jk}\alpha_{il}.$$

In other words, we can write the Hessian matrix $H_p(n_p)$ in the orthonormal basis $\nabla_p x_i$ as $(\alpha_{ij})_{i,j}$. The simpler Ricci and scalar curvatures are defined using R as

$$\operatorname{Ric}_{ij} = \sum_{k=1}^{d} R_{kikj} = \sum_{k=1}^{d} (\alpha_{kk}\alpha_{ij} - \alpha_{ik}\alpha_{jk})$$

and

$$S = \sum_{i=1}^{d} \operatorname{Ric}_{ii} = \sum_{i,j=1}^{d} R_{ijij} = 2 \sum_{i < j} (\alpha_{ii} \alpha_{jj} - \alpha_{ij}^{2}).$$

Hypersurfaces that are orientable also have a generalised notion of Gaussian curvature, given by $\kappa = \det(H_p(n_p))$. Note that, when d = 2, $S = 2(\alpha_{11}\alpha_{22} - \alpha_{12}^2) = 2\kappa$, but in all other dimensions the scalar and Gaussian curvature are not proportional.

We can simplify the above expressions by diagonalising the Hessian $H_p(n_p)$ to get an orthonormal basis for $T_p\mathcal{M}$ of eigenvectors $\nabla_p x_i$ with eigenvalues λ_i , so now $\alpha_{ij} = \lambda_i \delta_{ij}$. We call the λ_i the principal curvatures and the $\nabla_p x_i$ the principal curvature directions. The formula for the Riemann curvature now becomes

$$R_{ijkl} = \begin{cases} \lambda_i \lambda_j & \text{if } i = k \neq j = l \\ -\lambda_i \lambda_j & \text{if } i = l \neq j = k \\ 0 & \text{otherwise} \end{cases}$$

and the Ricci curvature becomes

$$\operatorname{Ric}_{ij} = \sum_{k=1}^{d} (\lambda_k \lambda_i \delta_{ij} - \lambda_i \lambda_j \delta_{ik} \delta_{jk}) = (\lambda_i \sum_{k \neq i} \lambda_k) \delta_{ij}.$$

Notice that this expression is diagonal, so the Ricci curvature has the same eigenvectors as $H_p(n_p)$ (the principal curvature directions). The scalar curvature is

$$S = 2\sum_{i < j} \lambda_i \lambda_j.$$

In the special case of surfaces, we get $Ric = \lambda_1 \lambda_2 I$ and $S = 2\lambda_1 \lambda_2$.

2.3 Curvature of general manifolds

In the general case, when \mathcal{M} is not a hypersurface, we have a (D-d)-dimensional normal space at each point $p \in \mathcal{M}$. If \vec{n}_p^{ℓ} , $\ell = 1, ..., D-d$ is an orthonormal basis for the normal space at p, and X, Y are vector fields, we define the second fundamental form at p to be the vector

$$\mathbb{I}_{p}(X,Y) = \sum_{\ell=1}^{D-d} H_{p}(n_{p}^{\ell})(X,Y)\vec{n}_{p}^{\ell}.$$

The Gauss equation now reads

$$\begin{split} g(R(X,Y)Z,W)(p) &= \mathbb{I}_p(X,Z) \cdot \mathbb{I}_p(Y,W) - \mathbb{I}_p(Y,Z) \cdot \mathbb{I}_p(X,W) \\ &= \sum_{\ell=1}^{D-d} \left[H_p(n_p^\ell)(X,Z) H_p(n_p^\ell)(Y,W) - H_p(n_p^\ell)(Y,Z) H_p(n_p^\ell)(X,W) \right]. \end{split}$$

We can therefore apply the same analysis as before to each unit normal \vec{n}_p^{ℓ} separately, and then sum them up. Writing the Hessian $H_p(n_p^{\ell})(\nabla_p x_i, \nabla_p x_j) = (\alpha_{ij}^{\ell})_{i,j}$, we obtain the Riemann

$$R_{ijkl} = \sum_{\ell=1}^{D-d} (\alpha_{ik}^{\ell} \alpha_{jl}^{\ell} - \alpha_{jk}^{\ell} \alpha_{il}^{\ell}),$$

Ricci

$$\operatorname{Ric}_{ij} = \sum_{\ell=1}^{D-d} \sum_{k=1}^{d} (\alpha_{kk}^{\ell} \alpha_{ij}^{\ell} - \alpha_{ik}^{\ell} \alpha_{jk}^{\ell}),$$

and scalar curvatures

$$S = \sum_{\ell=1}^{D-d} \sum_{i,j=1}^{d} (\alpha_{ii}^{\ell} \alpha_{jj}^{\ell} - (\alpha_{ij}^{\ell})^{2}).$$

These equations hold whatever choice of orthonormal basis n_p^{ℓ} we made.

3 Computing the dimension, tangent space, and curvature

Suppose $\mathcal{M} \subseteq \mathbb{R}^D$ is a d-dimensional submanifold of \mathbb{R}^D and $\{p_1, ..., p_n\} \subset \mathcal{M}$ is a sample of data from \mathcal{M} . We now outline an approach to computing the dimension d, the tangent spaces $T_{p_i}\mathcal{M}$, and the Riemann, Ricci, and scalar curvatures.

The code is available at https://github.com/Iolo-Jones/ManifoldDiffusionGeometry.

3.1 Diffusion maps and diffusion geometry

The geometry of \mathcal{M} is captured by its Riemannian metric g, which we can access through the 'carré du champ' formula

$$g(\nabla f, \nabla h) = \frac{1}{2} (f\Delta(h) + h\Delta(f) - \Delta(fh)), \tag{1}$$

which expresses the Riemannian metric of the vector fields ∇f and ∇h in terms of the Laplacian Δ . Our strategy will be to estimate Δ from the data, then use the carré du champ formula to compute the first and second fundamental forms. This approach (called *diffusion geometry*) was developed extensively in [25] where we used the carré du champ to develop a theory of differential geometry for general probability

spaces and data sampled from them; here we apply those methods to the special case of data from manifolds.

Let $X = \{p_1, ..., p_n\}$ be our sample of n data. If $A = \{f : X \to \mathbb{R}\}$ is the algebra of functions on X, we can identify $A \cong \mathbb{R}^n$ where the unit vector $e_i \in \mathbb{R}^n$ corresponds to the function $f(p_j) = \delta_{ij}$. There is a vast body of work on the problem of estimating Δ from X, and we will use the diffusion maps method [13] which forms a normalised heat kernel matrix from X to estimate Δ on a compact manifold. In other words, we compute the $n \times n$ matrix

$$K_{\epsilon}(x_i, x_j) = \exp\left(-\frac{||x_i - x_j||^2}{\epsilon}\right)$$

for all i, j and bandwidth parameter ϵ , and use it to construct an estimate $\hat{\Delta}_{\epsilon}$ for Δ . In other words, $\hat{\Delta}_{\epsilon}$ is an $n \times n$ matrix such that, if $f \in C^3(\mathcal{M})$ and \hat{f} is the vector $\hat{f}_i = f(p_i)$, then, up to rescaling $\hat{\Delta}_{\epsilon}$ by a constant positive factor, $(\hat{\Delta}_{\epsilon}\hat{f})_i \approx \Delta(f)(p_i)$. The use of the heat kernel means that this method is very robust to noise. We will specifically use variable bandwidth diffusion kernels [8] of the form

$$K_{\epsilon}(x_i, x_j) = \exp\left(-\frac{||x_i - x_j||^2}{\epsilon \rho(x)\rho(y)}\right),$$

where ρ is an automatically defined bandwidth function, which further improve performance and generalise the method to the non-compact case. We will use the estimate $\hat{\Delta}_{\epsilon}$ given in [8], where the authors show the following convergence result.

Theorem 3.1 (From Corollary 1, [8]). Let $q \in L^1(\mathcal{M}) \cap C^3(\mathcal{M})$ be a density that is bounded above on \mathcal{M} and let X be sampled independently with distribution q. If $f \in L^2(\mathcal{M}, q) \cap C^3(\mathcal{M})$ is a smooth function, \hat{f} is the vector $\hat{f}_i = f(p_i)$, and $p_i \in X$ is an arbitrary point then, with high probability,

$$(\hat{\Delta}_{\epsilon}\hat{f})_{i} = \Delta(f)(p_{i}) + \mathcal{O}\left(\epsilon, \frac{q(p_{i})^{1/2 + d/4}}{\sqrt{n}\epsilon^{2 + d/4}}, \frac{||\nabla_{p_{i}}f||q(p_{i})^{d^{2}/2 - 5d/4 + 1}}{\sqrt{n}\epsilon^{1/2 + d/4}}\right)$$

up to rescaling $\hat{\Delta}_{\epsilon}$ by a constant positive factor c.

Crucially, this estimate is normalised to be independent of the sampling density q, so we accurately recover Δ even when the data are not uniformly sampled from \mathcal{M} . There is a straightforward procedure for automatically selecting ϵ which we also adopt from [8], so obtain a parameter-free estimate $\hat{\Delta}$.

This result is notable when the data does not actually lie on a manifold. Manifolds are locally homeomorphic to Euclidean space everywhere, and the dimension of that Euclidean space must be constant everywhere. Real data, on the other hand, may only be locally homeomorphic to Euclidean space in some areas, and its dimension might jump around. The pointwise convergence of Theorem 3.1 ensures that, in this (more realistic) situation, the dimension, tangent space, and curvature estimates defined here will still make sense locally if not globally.

We can use $\hat{\Delta}$ to estimate the carré du champ by plugging it into the formula (1). If we let $\Gamma(f,h) = g(\nabla f, \nabla h)$ denote the 'carré du champ operator', we can estimate

$$\hat{\Gamma}(\hat{f}, \hat{h}) = \frac{1}{2} (\hat{f} \hat{\Delta} \hat{h} + \hat{h} \hat{\Delta} \hat{f} - \hat{\Delta} (\hat{f} \hat{h})) \approx \Gamma(f, h).$$

We can apply Theorem 3.1 to obtain a nearly identical pointwise convergence result for $\hat{\Gamma}$, provided $f, h, fh \in L^2(\mathcal{M}, q) \cap C^3(\mathcal{M})$.

3.2 Metric and dimension

We can use the estimate for the carré du champ to compute the dimension d of \mathcal{M} and tangent spaces $T_p\mathcal{M}$. Notice that the gradients of the ambient coordinate functions $\{\nabla_p x_i : i = 1, ..., D\}$ will span $T_p\mathcal{M}$ at each $p \in \mathcal{M}$. The Riemannian metric gives an inner product in $T_p\mathcal{M}$, and we can form the following $D \times D$ Gram matrix G(p) of inner products for the gradients of the coordinate functions:

$$G(p) = \begin{pmatrix} g(\nabla_p x_1, \nabla_p x_1) & \dots & g(\nabla_p x_1, \nabla_p x_D) \\ \dots & & \dots \\ g(\nabla_p x_D, \nabla_p x_1) & \dots & g(\nabla_p x_D, \nabla_p x_D) \end{pmatrix} = \begin{pmatrix} \Gamma(x_1, x_1) & \dots & \Gamma(x_1, x_D) \\ \dots & & \dots \\ \Gamma(x_D, x_1) & \dots & \Gamma(x_D, x_D) \end{pmatrix}$$

This matrix is symmetric and has rank d at every p (since $T_p\mathcal{M}$ is d-dimensional), so has d positive eigenvalues whose eigenvectors form an orthonormal basis for $T_p\mathcal{M}$. The fact that \mathcal{M} is isometrically embedded means that those positive eigenvalues will all be 1. The other D-d eigenvectors (with eigenvalue 0) form an orthonormal basis for the 'normal space' of vectors orthogonal to $T_p\mathcal{M}$.

3.2.1 Tangent space estimation

We can use our estimate $\hat{\Gamma}$ for the carré du champ Γ to form an estimate $\hat{G}(p_i)$ of $G(p_i)$, i.e. we compute a $D \times D$ matrix $\hat{G}(p_i)$. If we then diagonalise $\hat{G}(p_i)$, its D eigenvectors will form an orthonormal basis for \mathbb{R}^D and the first d of those should form an orthonormal basis for $T_{p_i}M$.

3.2.2 Normalisation

Recall that the diffusion maps Laplacian $\hat{\Delta}$ gives an estimate for Δ up to rescaling by a constant positive factor c, which will also lead to $\hat{\Gamma}$ and \hat{G} being rescaled by c. We can correct this using the fact that the first d eigenvalues $\lambda_1^i, ..., \lambda_d^i$ of the matrix $G(x_i)$ should be 1, but the eigenvalues $\hat{\lambda}_1^i, ..., \hat{\lambda}_d^i$ we estimate from \hat{G} are rescaled to c. So we can estimate c by computing the mean eigenvalue at each point p_i and then taking the median over i,

$$\hat{c} = \operatorname{median} \Big\{ \frac{1}{d} \sum_{i=1}^{d} \hat{\lambda_{j}^{i}} : i = 1, ..., n \Big\}.$$

We then rescale $\hat{\Delta}$ and $\hat{\Gamma}$ by $1/\hat{c}$.

3.2.3 Dimension estimation

If we do not know d in advance, we can estimate it from the eigenvalues of the $\hat{G}(p_i)$ given that, if $\hat{\lambda}_{\ell}^i$ is the ℓ^{th} largest eigenvalue of $\hat{G}(p_i)$, we expect

$$\hat{\lambda}_{\ell}^{i} \approx \begin{cases} c & \ell \leq d \\ 0 & \ell > d \end{cases}$$

for all i. We cannot estimate c as described in 3.2.2 without knowing d, so will now just assume that c = 1, which seems perfectly sufficient in practice. If we form the vector of differences

$$D_i = (1 - \hat{\lambda}_1^i, \hat{\lambda}_1^i - \hat{\lambda}_2^i, \hat{\lambda}_2^i - \hat{\lambda}_3^i, ..., \hat{\lambda}_{D-1}^i - \hat{\lambda}_D^i, \hat{\lambda}_D^i)$$

then D_i should be 1 in the d^{th} entry and zero elsewhere, so we can estimate the dimension at the point p_i to be

$$\hat{d}(i) = \operatorname{argmax} D_i. \tag{2}$$

Notice that the c=1 assumption only affects \hat{d} where the data are 0-dimensional. When the data lies on a manifold, $\hat{d}(i)$ should equal d everywhere. More generally, given that $\hat{d}(i)$ is derived from the heat diffusion operator, we can think of it as measuring the number of independent directions through which heat can flow along the data through x_i . We can obtain a global dimension estimate \hat{d} from the pointwise one $\hat{d}(i)$ by taking the median over all i.

3.3 Curvature

We have now obtained estimates for the tangent bundle, normal bundle, and carré du champ, and can use these to compute the curvature. To ease the notation, we will describe the computation at a given point $p = p_i$, and drop the index where possible.

The eigenvectors of $\hat{G}(p)$ form an orthonormal basis for \mathbb{R}^D : the first d approximate an orthonormal basis $\nabla_p x_1, ..., \nabla_p x_d$ for $T_p \mathcal{M}$, and the last D-d approximate normal vectors $\vec{n}^1, ..., \vec{n}^{D-d}$. To compute the curvature at p, we would like to compute the Hessian terms $\alpha_{ij}^{\ell} = H_p(n^{\ell})(\nabla_p x_i, \nabla_p x_j)$ for each normal vector n^{ℓ} and all pairs of tangent vectors $\nabla_p x_i, \nabla_p x_j$. We can write α_{ij}^{ℓ} in terms of the carré du champ, via the formula¹

$$H(f)(\nabla h_1, \nabla h_2) = \frac{1}{2} \big(\Gamma(h_1, \Gamma(h_2, f)) + \Gamma(h_2, \Gamma(h_1, f)) - \Gamma(f, \Gamma(h_1, h_2)) \big),$$

 $^{^{1}}$ This formula is well-known in the theory of Markov diffusion operators: see [7] for a survey and Proposition 9.1. in [25] for a derivation.

and so use $\hat{\Gamma}$ to compute estimates $\hat{\alpha}_{ij}^{\ell}$ for α_{ij}^{ℓ} . We then get estimators for the Riemann

$$\hat{R}_{ijkl} = \sum_{\ell=1}^{D-d} (\hat{\alpha}_{ik}^{\ell} \hat{\alpha}_{jl}^{\ell} - \hat{\alpha}_{jk}^{\ell} \hat{\alpha}_{il}^{\ell}),$$

Ricci

$$\hat{\mathrm{Ric}}_{ij} = \sum_{\ell=1}^{D-d} \sum_{k=1}^{d} (\hat{\alpha}_{kk}^{\ell} \hat{\alpha}_{ij}^{\ell} - \hat{\alpha}_{ik}^{\ell} \hat{\alpha}_{jk}^{\ell}),$$

and scalar curvatures

$$\hat{S} = \sum_{\ell=1}^{D-d} \sum_{i,j=1}^{d} (\hat{\alpha}_{ii}^{\ell} \hat{\alpha}_{jj}^{\ell} - (\hat{\alpha}_{ij}^{\ell})^{2}).$$

The Hessian estimates $\hat{\alpha}_{ij}^{\ell}$ involve the terms $\hat{\Delta}^2$, and so Theorem 3.1 guarantees pointwise convergence at p as long as x_i , n^{ℓ} , $x_i x_j$, $x_i n^{\ell}$, $x_i \Delta(x_j n^{\ell})$, $n^{\ell} \Delta(x_i x_j)$, and $\Delta(x_i x_j n^{\ell})$ are all in $L^2(\mathcal{M}, q) \cap C^3(\mathcal{M})$.

4 Dimension estimation

4.1 Pointwise dimension

We defined an estimate $\hat{d}(i)$ at a point x_i in equation (2) as the rank of the metric, or, more generally, as the number of independent directions that heat can flow through x_i . This diffusion dimension varies across the data and measures the effective dimension of the space at every point. When the data are drawn from a manifold \mathcal{M} without boundary, $\hat{d}(i)$ should be constant. When the data lie on manifolds with boundaries and corners, or on the union of several manifolds (which are examples of stratified spaces), $\hat{d}(i)$ can vary and encode interesting local geometry, which we see in Figure 2.

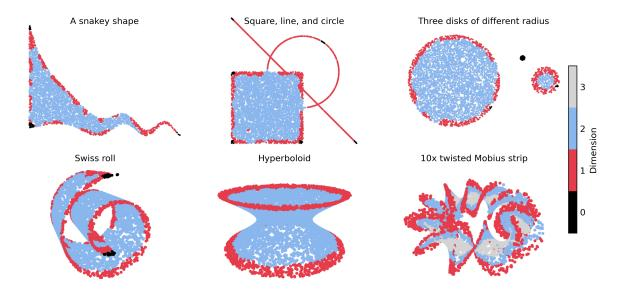


Figure 2: **Pointwise diffusion dimension.** The dimension is estimated at each point for data in 2d (top row) and 3d (bottom row). This process generally identifies 1-dimensional boundaries as 1-dimensional, and hard corners as 0-dimensional. These examples are given without noise for clarity, although this process is very robust to noise.

4.2 Global dimension

The problem of manifold dimension estimation is very well-studied, and we can define a global dimension estimate \hat{d} as the median of $\hat{d}(i)$ across the data. To test the accuracy of \hat{d} , we sample data from the 1,2, and 3-dimensional manifolds in the challenging dimension estimation benchmark proposed in [9]. We

add to this benchmark the 1, 2, and 3-dimensional hyperspheres and tori, as well as the 2-dimensional hyperboloid, embedded in a variety of ambient dimensions². This results in 12 test manifolds, including deliberately difficult examples with high curvature, such as the 10-times twisted Möbius strip in Figure 2, and tightly-wound helices. We focus on at most 3-dimensional data for the reasons outlined in the introduction. For each manifold, we sample n data where either $n = n_{small}$ or $n = n_{large}$, where n_{small} and n_{large} vary with dimension³. We also add normally distributed noise with standard devition 0, $0.5\sigma_{max}$, or σ_{max} , where σ_{max} is defined separately for each manifold in the benchmark as the largest value such that at least one method can attain at least 50% accuracy with that much noise.

We test the diffusion geometry estimate \hat{d} on this challenging data, against eleven standard and state-of-the-art methods, Correlation Dimension [19], Dimensionality from Angle and Norm Concentration (DANCo) [11], Expected Simplex Skewness (ESS) [24], Fisher Separability [3], local principal component analysis (LPCA) [10, 16, 18], Manifold-Adaptive Dimension Estimation (MADA) [17], Minimum Neighbor Distance - Maximum Likelihood (MiND-ML) [29], Maximum Likelihood Estimation (MLE) [20, 22, 26], Method of Moments (MOM) [4], Tight Local intrinsic dimensionality Estimator (TLE) [5], and Two Nearest Neighbours (TwoNN) [15]. Some of these methods return non-integer dimension estimates, and in these cases we round to the nearest integer. Most of these methods also have parameters to be set, but, to fairly test their real-world performance, these parameters are all set to their default values, as implemented in [6]. We measure the average accuracy of each method across 20 samples of each of the 12 manifolds in the benchmark, for the different numbers of data n and levels of noise σ , and record the results in Table 1.

	$n = n_{small}$			$n = n_{large}$			
Method	$\sigma = 0$	$\sigma = 0.5\sigma_{max}$	$\sigma = \sigma_{max}$	$\sigma = 0$	$\sigma = 0.5\sigma_{max}$	$\sigma = \sigma_{max}$	
Correlation Dimension [19]	$\boxed{\textbf{100.0} \pm \textbf{0.0}}$	$\textbf{87.1} \pm \textbf{6.6}$	21.2 ± 4.1	91.7 ± 0.0	35.8 ± 7.5	5.8 ± 3.8	
MADA [17]	91.7 ± 0.0	32.9 ± 11.5	0.0 ± 0.0	91.7 ± 0.0	8.3 ± 0.0	0.0 ± 0.0	
LPCA [10, 16, 18]	8.3 ± 0.0	8.3 ± 0.0	0.0 ± 0.0	8.3 ± 0.0	8.3 ± 0.0	0.0 ± 0.0	
MLE [20, 22, 26]	91.7 ± 0.0	47.1 ± 6.3	0.0 ± 0.0	91.7 ± 0.0	17.1 ± 1.8	0.0 ± 0.0	
MiND-ML [29]	92.1 ± 1.8	18.3 ± 3.3	0.0 ± 0.0	100.0 ± 0.0	17.1 ± 1.8	0.4 ± 1.8	
DANCo [11]	91.7 ± 0.0	0.0 ± 0.0	0.0 ± 0.0	98.8 ± 3.0	0.4 ± 1.8	0.0 ± 0.0	
TwoNN [15]	100.0 ± 0.0	11.2 ± 5.6	7.9 ± 1.8	100.0 ± 0.0	8.3 ± 0.0	8.3 ± 0.0	
MOM[4]	75.0 ± 0.0	66.7 ± 0.0	$\textbf{50.0} \pm \textbf{0.0}$	83.3 ± 0.0	$\textbf{73.3} \pm \textbf{3.3}$	20.8 ± 4.2	
Fisher Separability [3]	16.7 ± 0.0	16.7 ± 0.0	15.4 ± 3.0	16.7 ± 0.0	16.7 ± 0.0	15.0 ± 3.3	
TLE [5]	91.7 ± 0.0	0.0 ± 0.0	0.0 ± 0.0	91.7 ± 0.0	0.0 ± 0.0	0.0 ± 0.0	
Diffusion Geometry	88.8 ± 4.0	83.3 ± 0.0	55.0 ± 7.7	90.8 ± 2.5	$\textbf{79.6} \pm \textbf{4.1}$	58.8 ± 11.0	

Table 1: Manifold dimension estimation. Average accuracies and standard deviations (%) from 20 runs over 12 benchmark manifolds with dimensions 1, 2, and 3. The standard deviations are computed for each manifold and then averaged overall, so 0 means that the method returned the same value for each manifold on every run. We sample n data randomly for a small and large value of n, and for zero, medium, and large amounts of noise. The red and blue numbers indicate the best and second-best accuracies in each column.

The many methods tested here all respond to noise and density in different ways: some achieve outstanding accuracy on clean data but have virtually no robustness to noise (MADA, MLE, MiND-ML, DANCo, TwoNN, TLE), and many performed especially well on one or two particular examples in the benchmark. Overall, the best-performing methods across the test are clearly correlation dimension, method of moments (MOM), and diffusion geometry. Correlation dimension is highly accurate on clean data and also reasonably robust, but only at the lower density n_{small} . MOM is more robust, and deals better with the change in density, but is overall less accurate. Diffusion geometry, while not the most accurate method for perfect, noiseless data, is by far the most robust to noise and density, and achieves the highest accuracy of any model in 3 of the 4 noisy examples.

Low-dimensional data are often encountered in a very high-dimensional ambient space, but we find this does not significantly affect the performance or robustness of these methods. Running the same test on

²The results on the benchmark of [9] alone are in the Appendix, and are qualitatively very similar.

³When d=1, $n_{small}=600$ and $n_{large}=1200$, when d=2, $n_{small}=1200$ and $n_{large}=2400$, and when d=3, $n_{small}=2400$ and $n_{large}=4800$.

the same data but embedded in a range of higher ambient dimensions does not change the results.

5 Tangent space estimation

In Subsection 3.2.1, we used the leading eigenvectors of the metric as an approximate basis for the tangent space $T_{x_i}\mathcal{M}$ of a manifold \mathcal{M} . When the data lie on 'manifold-like' objects such as the union of manifolds, this 'tangent space' estimate encodes something like the directions of strongest diffusion through the space. We compute the 1 and 2-dimensional tangent spaces of noisy data in Figure 3.

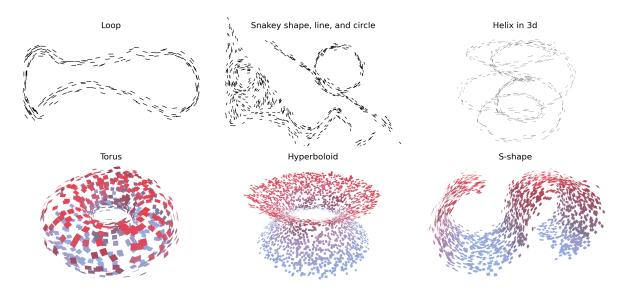


Figure 3: **Tangent spaces of data.** We compute the 1d (top row) and 2d (bottom row) tangent space for each point. When the data are from a manifold, we robustly recover the tangent bundle even with large amounts of noise. When the data is not a manifold (top centre example), these 'diffusion tangents' measure the direction of greatest heat flow along the object.

The standard technique for this task is local principal component analysis (LPCA), which, for some given parameter k, computes the covariance matrix of the k-nearest neighbours to each point x_i , and defines the tangent space to be its leading d eigenvectors. In other words, it performs principal component analysis in a neighbourhood of each point, so follows the hard neighbourhood paradigm. LPCA can be effective in many situations but depends sensitively on the choice of neighbourhood size k, whose optimal value depends on the amount of noise, density of the sample, and geometry of the underlying manifold. When k is small, LPCA can accurately compute the tangent space for clean data but is extremely sensitive to noise. When k is large, LPCA becomes much more noise-robust but is only accurate on very dense samples. This trade-off is inherent to hard neighbourhood methods.

Conversely, the diffusion geometry tangent space estimator does not need parameter selection and is highly robust to both noise and density simultaneously. To compare the two methods, we sample data from the torus in Figure 3 with different densities and noise levels. We estimate the tangent space with diffusion geometry and LPCA with two neighbourhood parameters: k = 5 and k = 100. To test the accuracy of an estimate at point x_i , we compute the normal vector to the estimated tangent plane, and compare it with the correct normal to the torus at x_i (or at the point on the torus closest to x_i , when the data contains noise). We then compute the angle between these two normal vectors and average it over the data: when the average is 0° the estimator is perfectly accurate, and when the average is over 45° the tangent spaces are essentially random. We visualise the results in Figure 4.

We find that, while LPCA can always attain very high accuracy with near-perfect data, no fixed value of k is robust to both noise and density. Conversely, the diffusion geometry tangents attain comparable accuracy for high-density and low-noise data but can maintain good accuracy even when the data is low-density and highly noisy. In particular, diffusion geometry outperforms LPCA with either parameter when n < 1000 and especially when $\sigma > 0.02$. The torus data in Figure 3 has n = 600 and $\sigma = 0.1$ so

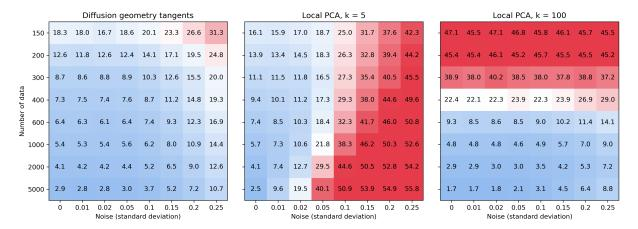


Figure 4: **Diffusion Geometry vs Local PCA.** We compute the tangent space for a torus in \mathbb{R}^3 with different sampling densities and noise levels, using tangent diffusion and LPCA. We measure accuracy at a point by finding the 'error angle' between the normal vector to the computed tangent space and the true normal at that point. The grids contain the average error angle in degrees, averaged over 10 runs: 0° means perfect accuracy over the whole torus and over 45° means the tangent spaces are random. LPCA is computed for k=5 and k=100 nearest neighbours: both values perform well in places but no fixed value of k is always good. Diffusion geometry is comparable to or better than LPCA and does not need parameter selection.

is right on this boundary: it is clearly a torus to the human eye but is hard for LPCA. For geometric analysis of real data, it is especially important to perform well on exactly this sort of low-quality, sparse and noisy data.

6 Curvature estimation

6.1 Scalar curvature

In Subsection 3.3, we introduced estimators for the Riemann, Ricci, and scalar curvatures using the second fundamental form defined by the Hessian. These give us a powerful description of the local geometry of manifolds. We give several examples of the scalar curvature of a surface in Figure 5.

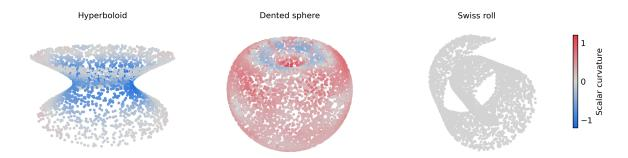


Figure 5: Scalar curvature of surfaces. We compute the scalar curvature with diffusion geometry. When the surface is locally spherical, the curvature is positive (e.g. on most of the dented sphere). When the surface is locally hyperbolic the curvature is negative (e.g. the hyperboloid, which is negatively curved everywhere, and the 'rim' of the dent on the sphere). Zero curvature means the surface looks like Euclidean space, such as on the Swiss roll, which is a wrapped but, crucially, not deformed rectangle.

We test our estimate on challenging, low-quality data by sampling points from a torus in \mathbb{R}^3

$$\{ ((R + r\cos(\phi))\cos(\theta), (R + r\cos(\phi))\sin(\theta), r\sin(\theta)) : \phi, \theta \in [0, 2\pi) \}$$

(we choose r=1 and R=2) and comparing the estimated scalar curvature to the correct value

$$S(\theta, \phi) = \frac{2\cos(\phi)}{r(R + r\cos(\phi))}.$$
(3)

Notice that S depends only on the internal angle ϕ , so in Figure 6 we plot our estimate against 'ground truth' as functions of ϕ . Even with noisy and low-density data, our estimator is very accurate.

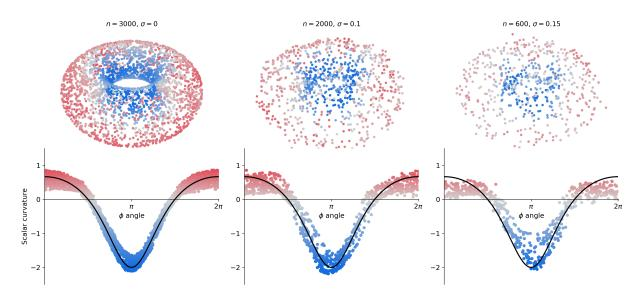


Figure 6: Diffusion scalar curvature vs ground truth. We compute scalar curvature on a torus using diffusion geometry (top row) and compare it to the true scalar curvature (bottom row). The true curvature (3) depends only on the internal angle ϕ of the torus, and is plotted in black alongside the diffusion geometry estimate. When the data contain noise, the estimated curvature at x_i is plotted against the ϕ value of the point on the torus closest to x_i .

There have been, to our knowledge, only two previous attempts to estimate the scalar curvature on a general manifold. Sritharan, Wang and Hormoz (SWH) [32] estimated the scalar curvature using a similar extrinsic approach to the one described above, but used local linear and quadratic regression to estimate the tangent spaces and Hessian. More recently, Hickok and Blumberg (HB) [21] presented a method based on the volume comparison properties of the scalar curvature. There are also several surface-specific methods for computing scalar curvature, which generally follow a similar approach to the SWH curvature, and, in our experiments, do not perform better than it, so are not presented here.

Since the SWH curvature also follows the *hard neighbourhood paradigm* of estimating differential objects through local regression in a neighbourhood, it comes with a parameter that controls neighbourhood size. SWH uses a 'standard error' parameter that lets the user control the target precision of the method: smaller values are more precise but less robust. Conversely, the diffusion geometry scalar curvature is not parameterised and does not have to make the *hard neighbourhood* trade-off between accuracy and robustness. The HB approach is intrinsic, so does not need an embedding of the data, but, in our experiments, is significantly less accurate than the other two methods.

We compare the diffusion geometry and SWH scalar curvatures by the same experiment as in Figure 4: sampling data from a torus and comparing the computed estimates to ground truth. We use two different values of standard error parameter, 0.02 and 0.1, in the SWH method. We average the results over 10 runs and present them in Figure 7.

Just like LPCA, the SWH curvature attains very high accuracy with near-perfect data, but there is a significant trade-off between accuracy and robustness to noise and density. Conversely, the diffusion

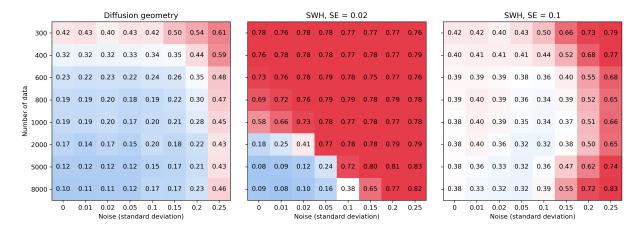


Figure 7: Diffusion geometry vs Sritharan/Wang/Hormoz scalar curvature. We compute the scalar curvature of a torus in \mathbb{R}^3 with different sampling densities and noise levels, using diffusion geometry and the SWH method. We compare the estimates to the true scalar curvature (3) and record the mean absolute error averaged over 10 runs. The SWH curvature is computed for the standard error parameters 0.02 and 0.1: this choice presents a trade-off between accuracy and robustness. Diffusion geometry does not need parameter selection and attains comparable performance on perfect data, but deals significantly better with noise and sparsity.

geometry scalar curvature has comparable accuracy for high-density and low-noise data but still performs very well when the data is sparse and noisy. The two noisy examples in Figure 6 are much too sparse and noisy for SWH, but can be computed very accurately with diffusion geometry.

Even though the diffusion geometry method presented here is manifold-specific, these strong statistical results suggest that it could provide meaningful curvature analysis on real-world data.

6.2 Ricci and Riemann curvature

The Ricci curvature only differs from the scalar curvature in dimension 3. The papers [1] and [2] describe an estimator for it, but do not test it on data. We tested the Ricci estimate given in Subsection 3.3 on several examples, but obtaining a high enough density to really observe its deviation from the scalar curvature requires n to be huge. We could not find any interesting examples where n < 50,000, which is too large to be practical.

The Riemann curvature only differs from the Ricci in dimension 4, where obtaining a sufficiently dense sample to notice the difference is infeasible.

7 Conclusions

We have introduced a range of novel computational geometry tools for data on manifolds, based on diffusion geometry. While these new methods attain comparable results to the existing state-of-the-art on low-noise, dense data, they significantly outperform existing methods in the presence of noise or sparsity.

We have consistently found that methods that follow the *hard neighbourhood paradigm* must trade off precision against robustness, and come with a user-defined parameter to control this. Even the optimal choice of this parameter is usually not enough to attain high accuracy on very sparse and noisy data. Conversely, diffusion geometry is not a *hard neighbourhood* method, so enjoys both accuracy and robustness simultaneously while also being parameter-free.

Important future research questions include: can we define and measure curvature on non-manifold data, and can local dimensionality and curvature measures work effectively as features for geometric machine learning?

Acknowledgements

I want to thank Jeff Giansiracusa and Yue Ren for their generous comments and feedback. This work was carried out as part of EPSRC grant EP/Y028872/1, *Mathematical Foundations of Intelligence: An "Erlangen Programme" for AI*.

Appendix: other dimension benchmark results

The benchmark used for the results in Table 1 included six manifolds from the benchmark proposed in [9], as well as six additional ones. For completeness, we include the results obtained *only on the benchmark data from* [9] in Table 2. There are seven manifolds in the benchmark from [9] of dimension at most 3, although one of these, the 'M13b Spiral', was too challenging for any of the methods considered to be accurate with any amount of noise, so is excluded.

		$n = n_{small}$			$n = n_{large}$	
Method	$\sigma = 0$	$\sigma = 0.5\sigma_{max}$	$\sigma = \sigma_{max}$	$\sigma = 0$	$\sigma = 0.5\sigma_{max}$	$\sigma = \sigma_{max}$
Correlation Dimension [19]	100.0 ± 0.0	$\textbf{75.8} \pm \textbf{8.3}$	16.7 ± 0.0	83.3 ± 0.0	32.5 ± 3.6	0.0 ± 0.0
MADA [17]	83.3 ± 0.0	20.8 ± 7.2	0.0 ± 0.0	83.3 ± 0.0	0.0 ± 0.0	0.0 ± 0.0
LPCA [10, 16, 18]	16.7 ± 0.0	16.7 ± 0.0	0.0 ± 0.0	16.7 ± 0.0	16.7 ± 0.0	0.0 ± 0.0
MLE [20, 22, 26]	83.3 ± 0.0	33.3 ± 0.0	0.0 ± 0.0	83.3 ± 0.0	0.8 ± 3.6	0.0 ± 0.0
MiND-ML [29]	84.2 ± 3.6	3.3 ± 6.7	0.0 ± 0.0	$\textbf{100.0} \pm \textbf{0.0}$	16.7 ± 0.0	0.8 ± 3.6
DANCo [11]	83.3 ± 0.0	0.0 ± 0.0	0.0 ± 0.0	97.5 ± 6.0	0.8 ± 3.6	0.0 ± 0.0
TwoNN [15]	100.0 ± 0.0	16.7 ± 0.0	15.8 ± 3.6	$\textbf{100.0} \pm \textbf{0.0}$	16.7 ± 0.0	16.7 ± 0.0
MOM[4]	50.0 ± 0.0	33.3 ± 0.0	16.7 ± 0.0	66.7 ± 0.0	46.7 ± 6.7	0.0 ± 0.0
Fisher Separability [3]	33.3 ± 0.0	33.3 ± 0.0	30.8 ± 6.0	33.3 ± 0.0	33.3 ± 0.0	30.0 ± 6.7
TLE [5]	83.3 ± 0.0	0.0 ± 0.0	0.0 ± 0.0	83.3 ± 0.0	0.0 ± 0.0	0.0 ± 0.0
Diffusion Geometry	77.5 ± 7.9	$\textbf{66.7} \pm \textbf{0.0}$	$\textbf{42.5} \pm \textbf{11.8}$	81.7 ± 5.0	66.7 ± 0.0	36.7 ± 16.0

Table 2: Manifold dimension estimation on the benchmark data from [9] only. Average accuracies and standard deviations (%) from 20 runs over 12 benchmark manifolds with dimensions 1, 2, and 3. The standard deviations are computed for each manifold and then averaged overall, so 0 means that the method returned the same value for each manifold on every run. We sample n data randomly for a small and large value of n, and for zero, medium, and large amounts of noise. The red and blue numbers indicate the best and second-best accuracies in each column.

References

- [1] Antonio G Ache and Micah W Warren. Ricci curvature and the manifold learning problem. *Advances in Mathematics*, 342:14–66, 2019.
- [2] Antonio G Ache and Micah W Warren. Approximating coarse ricci curvature on submanifolds of euclidean space. *Advances in Geometry*, 22(2):215–243, 2022.
- [3] Luca Albergante, Jonathan Bac, and Andrei Zinovyev. Estimating the effective dimension of large biological datasets using fisher separability analysis. In 2019 International Joint Conference on Neural Networks (IJCNN), pages 1–8. IEEE, 2019.
- [4] Laurent Amsaleg, Oussama Chelly, Teddy Furon, Stéphane Girard, Michael E Houle, Ken-ichi Kawarabayashi, and Michael Nett. Extreme-value-theoretic estimation of local intrinsic dimensionality. *Data Mining and Knowledge Discovery*, 32(6):1768–1805, 2018.
- [5] Laurent Amsaleg, Oussama Chelly, Michael E Houle, Ken-ichi Kawarabayashi, Miloš Radovanović, and Weeris Treeratanajaru. Intrinsic dimensionality estimation within tight localities. In *Proceedings* of the 2019 SIAM international conference on data mining, pages 181–189. SIAM, 2019.
- [6] Jonathan Bac, Evgeny M Mirkes, Alexander N Gorban, Ivan Tyukin, and Andrei Zinovyev. Scikit-dimension: a python package for intrinsic dimension estimation. *Entropy*, 23(10):1368, 2021.

- [7] Dominique Bakry, Ivan Gentil, Michel Ledoux, et al. Analysis and geometry of Markov diffusion operators, volume 103. Springer, 2014.
- [8] Tyrus Berry and John Harlim. Variable bandwidth diffusion kernels. Applied and Computational Harmonic Analysis, 40(1):68–96, 2016.
- [9] Paola Campadelli, Elena Casiraghi, Claudio Ceruti, and Alessandro Rozza. Intrinsic dimension estimation: Relevant techniques and a benchmark framework. *Mathematical Problems in Engineering*, 2015(1):759567, 2015.
- [10] Richard Cangelosi and Alain Goriely. Component retention in principal component analysis with application to cdna microarray data. *Biology direct*, 2:1–21, 2007.
- [11] Claudio Ceruti, Simone Bassis, Alessandro Rozza, Gabriele Lombardi, Elena Casiraghi, and Paola Campadelli. Danco: dimensionality from angle and norm concentration. arXiv preprint arXiv:1206.3881, 2012.
- [12] David Cohen-Steiner, Herbert Edelsbrunner, and John Harer. Stability of persistence diagrams. In *Proceedings of the twenty-first annual symposium on Computational geometry*, pages 263–271, 2005.
- [13] Ronald R. Coifman and Stéphane Lafon. Diffusion maps. Applied and Computational Harmonic Analysis, 21(1):5–30, 2006. Special Issue: Diffusion Maps and Wavelets.
- [14] Edelsbrunner, Letscher, and Zomorodian. Topological persistence and simplification. *Discrete & computational geometry*, 28:511–533, 2002.
- [15] Elena Facco, Maria d'Errico, Alex Rodriguez, and Alessandro Laio. Estimating the intrinsic dimension of datasets by a minimal neighborhood information. *Scientific reports*, 7(1):12140, 2017.
- [16] Mingyu Fan, Nannan Gu, Hong Qiao, and Bo Zhang. Intrinsic dimension estimation of data by principal component analysis. arXiv preprint arXiv:1002.2050, 2010.
- [17] Amir Massoud Farahmand, Csaba Szepesvári, and Jean-Yves Audibert. Manifold-adaptive dimension estimation. In *Proceedings of the 24th international conference on Machine learning*, pages 265–272, 2007.
- [18] Keinosuke Fukunaga and David R Olsen. An algorithm for finding intrinsic dimensionality of data. *IEEE Transactions on computers*, 100(2):176–183, 1971.
- [19] Peter Grassberger and Itamar Procaccia. Measuring the strangeness of strange attractors. *Physica D: nonlinear phenomena*, 9(1-2):189–208, 1983.
- [20] Gloria Haro, Gregory Randall, and Guillermo Sapiro. Translated poisson mixture model for stratification learning. *International Journal of Computer Vision*, 80:358–374, 2008.
- [21] Abigail Hickok and Andrew J Blumberg. An intrinsic approach to scalar-curvature estimation for point clouds. arXiv preprint arXiv:2308.02615, 2023.
- [22] Bruce M Hill. A simple general approach to inference about the tail of a distribution. *The annals of statistics*, pages 1163–1174, 1975.
- [23] Jonathan Ho, Ajay Jain, and Pieter Abbeel. Denoising diffusion probabilistic models. *Advances in neural information processing systems*, 33:6840–6851, 2020.
- [24] Kerstin Johnsson, Charlotte Soneson, and Magnus Fontes. Low bias local intrinsic dimension estimation from expected simplex skewness. *IEEE transactions on pattern analysis and machine intelligence*, 37(1):196–202, 2014.
- [25] Iolo Jones. Diffusion geometry. arXiv preprint arXiv:2405.10858, 2024.
- [26] Elizaveta Levina and Peter Bickel. Maximum likelihood estimation of intrinsic dimension. Advances in neural information processing systems, 17, 2004.

- [27] Uzu Lim, Harald Oberhauser, and Vidit Nanda. Tangent space and dimension estimation with the wasserstein distance. SIAM Journal on Applied Algebra and Geometry, 8(3):650–685, 2024.
- [28] Vanessa Robins. Towards computing homology from finite approximations. *Topology proceedings*, 24(1):503–532, 1999.
- [29] Alessandro Rozza, Gabriele Lombardi, Claudio Ceruti, Elena Casiraghi, and Paola Campadelli. Novel high intrinsic dimensionality estimators. *Machine learning*, 89:37–65, 2012.
- [30] Jascha Sohl-Dickstein, Eric Weiss, Niru Maheswaranathan, and Surya Ganguli. Deep unsupervised learning using nonequilibrium thermodynamics. In *International conference on machine learning*, pages 2256–2265. PMLR, 2015.
- [31] Yang Song, Jascha Sohl-Dickstein, Diederik P Kingma, Abhishek Kumar, Stefano Ermon, and Ben Poole. Score-based generative modeling through stochastic differential equations. arXiv preprint arXiv:2011.13456, 2020.
- [32] Duluxan Sritharan, Shu Wang, and Sahand Hormoz. Computing the riemannian curvature of image patch and single-cell rna sequencing data manifolds using extrinsic differential geometry. *Proceedings of the National Academy of Sciences*, 118(29):e2100473118, 2021.
- [33] Afra Zomorodian and Gunnar Carlsson. Computing persistent homology. In *Proceedings of the twentieth annual symposium on Computational geometry*, pages 347–356, 2004.